

Influences of short-term and long-term plasticity of memristive synapse on firing activity of neuronal network

Zhi-Jun Li(李志军)† and Jing Zhang(张晶)
Citation: Chin. Phys. B, 2024, 33 (**12**): 128701. DOI: 10.1088/1674-1056/ad84c5
Journal homepage: http://cpb.iphy.ac.cn; http://iopscience.iop.org/cpb

What follows is a list of articles you may be interested in

Dynamical behavior of memristor-coupled heterogeneous discrete neural networks with synaptic crosstalk

Minglin Ma(马铭磷), Kangling Xiong(熊康灵), Zhijun Li(李志军), and Shaobo He(贺少波)
Chin. Phys. B, 2024, 33 (**2**): 028706. DOI: 10.1088/1674-1056/aceee9

Dynamics and synchronization in a memristor-coupled discrete heterogeneous neuron network considering noise

Xun Yan(晏询), Zhijun Li(李志军), and Chunlai Li(李春来)
Chin. Phys. B, 2024, 33 (**2**): 028705. DOI: 10.1088/1674-1056/ad062c

Effect of short-term plasticity on working memory

Fan Yang(杨帆) and Feng Liu(刘锋)
Chin. Phys. B, 2023, 32 (**11**): 118706. DOI: 10.1088/1674-1056/acf03a

Synchronization coexistence in a Rulkov neural network based on locally active discrete memristor

Ming-Lin Ma(马铭磷), Xiao-Hua Xie(谢小华), Yang Yang(杨阳), Zhi-Jun Li(李志军), and Yi-Chuang Sun(孙义闯)
Chin. Phys. B, 2023, 32 (**5**): 058701. DOI: 10.1088/1674-1056/acb9f7

Pattern transition and regulation in a subthalamopallidal network under electromagnetic effect

Zilu Cao(曹子露), Lin Du(都琳), Honghui Zhang(张红慧), Yuzhi Zhao(赵玉枝), Zhuan Shen(申转), and Zichen Deng(邓子辰)
Chin. Phys. B, 2022, 31 (**11**): 118701. DOI: 10.1088/1674-1056/ac80ae

---

Influences of short-term and long-term plasticity of memristive synapse on firing activity of neuronal network

Zhi-Jun Li(李志军)[†] and Jing Zhang(张晶)

School of Automation and Electronic Information, Xiangtan University, Xiangtan 411105, *China*

(Received 11 July 2024; revised manuscript received 10 September 2024; accepted manuscript online 9 October 2024)

Synaptic plasticity can greatly affect the firing behavior of neural networks, and it specifically refers to changes in the strength, morphology, and function of synaptic connections. In this paper, a novel memristor model, which can be configured as a volatile and nonvolatile memristor by adjusting its internal parameter, is proposed to mimic the short-term and long-term synaptic plasticity. Then, a bi-neuron network model, with the proposed memristor serving as a coupling synapse and the external electromagnetic radiation being emulated by the flux-controlled memristors, is established to elucidate the effects of short-term and long-term synaptic plasticity on firing activity of the neuron network. The resultant seven-dimensional (7D) neuron network has no equilibrium point and its hidden dynamical behavior is revealed by phase diagram, time series, bifurcation diagram, Lyapunov exponent spectrum, and two-dimensional (2D) dynamic map. Our results show the short-term and long-term plasticity can induce different bifurcation scenarios when the coupling strength increases. In addition, memristor synaptic plasticity has a great influence on the distribution of firing patterns in the parameter space. More interestingly, when exploring the synchronous firing behavior of two neurons, the two neurons can gradually achieve phase synchronization as the coupling strength increases along the opposite directions under two different memory attributes. Finally, a microcontroller-based hardware system is implemented to verify the numerical simulation results.

Keywords: synaptic plasticity, memristive synapse, electromagnetic radiation, hidden attractor, phase synchronization

PACS: 87.19.ll, 87.19.lj, 05.45.Pq, 05.45.Xt **DOI:** 10.1088/1674-1056/ad84c5

1. Introduction

The central nervous system (CNS) is composed of hundreds of millions of neurons, each with abundant complex electrical activities related to information processing.[1] The study of neuronal firing activity can provide theoretical guidance for physiological applications in the treatment of epilepsy,[2] Parkinson's disease,[3] and other neurological and psychiatric disorders. In order to further reveal the functions of the brain and understand the underlying firing mechanisms of biological neurons, many simplified artificial neuron models have been derived from the classical Hodgkin–Huxley (HH) paradigm,[4] including Hindmarsh–Rose (HR) model,[5] Izhikevich model,[6] Fitzhugh–Nagumo model (FHN),[7] and Hopfield neural network (HNN),[8–10] just to name a few. Among them, the HR model stands out as one of the most prominent representatives and has been extensively studied. Zhang *et al.*[11] proposed a no-equilibrium HR neuron model and found the interesting phenomenon of hidden homogeneous extreme multistability. Ge *et al.*[12] explored the HR model driven by periodic high-low-frequency currents, and found that external high-low-frequency stimuli play an important role in the auto-regulation of neural firing patterns. Wu *et al.*[13] revealed that the appropriate Gaussian white noise can induce two asynchronous Hindmarsh–Rose neurons to converge to synchronization. These studies have provided great help for the development of neurodynamics.[14]

Memristor, as the fourth fundamental circuit element defined by a constitutive relationship between charge and magnetic flux, is originally proposed by Chua in 1971.[15] Due to their strong nonlinearity, memristors play a significant role in generating complex nonlinear dynamic behaviors,[16,17] such as, initial-dependent coexisting attractors,[18] transient dynamics,[19] antimonotonicity,[20] and hidden attractors.[21] Furthermore, due to their natural bionic properties, memristors are considered a perfect device to simulate neuron synapses.[22–24] For example, Yu *et al.*[25] developed a two-neuron network coupled by a memristive synapse, and their results show that the initial state of the memristive synapse can regulate the energy diversity in the network and achieve the energy balance in the transient state. Bao *et al.*[26] synthesized a memristor-coupled HR neuron network without equilibrium points, and they found that the coupling strength and initial conditions of the memristive channel can modulate the synchronization dynamics and energy diversity. Chen *et al.*[27] presented a memristor coupled homogeneous neuron network and investigated its coexisting and synchronous behaviors. Lin *et al.*[28] constructed an memristor-coupled asymmetric neuronal network using two asymmetric sub-neural networks, and observed the phenomena of infinitely wide hyperchaos and hyperchaotic multi-structure attractors.

[†]Corresponding author. E-mail: lizhijun@xtu.edu.cn

© 2024 Chinese Physical Society and IOP Publishing Ltd

When studying neuronal firing activity, it is necessary to consider the effects of its complex external electrophysiological environment. In particular, electromagnetic radiation has been reported to be highly correlated with collective behavior in neuronal physiological functions (e.g., spatiotemporal patterns,[29] and synchronous states[30]). By virtue of the constitutive relation of ideal flux-controlled memristors, they can sense the variations in external electromagnetic radiation surrounding neurons and produce the corresponding induced currents, thus effectively simulating the effects of external electromagnetic radiation.[31] Lai *et al*.[32] proposed a local active discrete memristor to simulate the effect of electromagnetic radiation on electrical activity of FHN neuron, and discovered that the increase of electromagnetic radiation can induce hyperchaotic firing. Vinaya *et al*.[33] explored the occurrence of absence seizures under the effect of electromagnetic radiation from a memristor, and their results indicate that electromagnetic radiation contributes to the suppression of the formation of disorienting seizure activity in the cortico–thalamic system.

There is evidence that the regular action of the brain needs to be balanced in several neuronal and synaptic features, one of which is synaptic plasticity.[34] Synaptic plasticity[35] is the capacity of synaptic transmission between neurons to be strengthened or weakened, which incorporates three important mechanisms: short-term synaptic plasticity, long-term synaptic plasticity and spike-time-dependent plasticity.[36] Synaptic plasticity plays a key role in learning, memory, and the development of neurological dysfunction.[37] Therefore, it is crucial to study the effects of synaptic plasticity on neuronal firing behavior. Madadi Asl *et al*.[38] found that spike-time-dependent plasticity (STDP) in synaptic plasticity can lead to multistability of the neuronal dynamics, and also explored the effects on the dynamic behaviors and synchronization properties of bi-neuronal networks with STDP.[39,40] Chen *et al*.[41] introduced two internal state variables 'forgetting rate' and 'retention' into the memristive device, allowing the memristor to capture forgetting behavior while possessing basic memristive properties. Zhou *et al*.[42] proposed a multi-parameter control circuit based on the forgetting memristor, and found that compared with non-volatile memristors, volatile memristors exhibited LTP characteristics more in line with biological synapses under this circuit. Chen *et al*.[43] simulated the plasticity of biological synapses by controlling the long-term and short-term weights of the forgetting synapse through changing the resistance of memristors, and found that forgetting synapses with long-term and short-term memories have multi-weight storage compared with traditional synapses. To further investigate the influence of synaptic plasticity on neuronal firing behavior, we explored the effect of synaptic plasticity on the firing activity of a neuron in our previous study,[44] and proposed a memory state-switchable memristor to model the autapse of an HR neuron. To further explore the effect of synaptic plasticity on the dynamics of a two-neuron network, a novel memristor is proposed to simulate the short-term and long-term synaptic plasticity in this study. A bi-neuron network model coupled by the memristor is developed, where the effect of electromagnetic radiation on both neurons is simulated by two ideal flux-controlled memristors. Numerical analysis reveals the hidden firing activities of the network when the system parameters and memory attributes of the memristive synapse vary. In addition, we explore the synchronous firing behavior of neurons under the influence of synaptic plasticity.

The remainder of this paper is arranged as follows. A memristor with short-term and long-term synaptic plasticity is proposed in Section 2, and its memory attributes are investigated. In Section 3, a 7D homogeneous neuron network model with electromagnetic radiation is established. In Section 4, firing activities of the network with respect to the coupling strength of the memristor and the strength of electromagnetic radiation are investigated under two different memory attributes of the coupling memristor. In Section 5, the effect of coupling strength on synchronization behavior is studied. In Section 6, hardware experiment is performed to verify the numerical results. Conclusions are drawn in the last section.

2. Memristor with configurable memory attributes

2.1. Memristor model

In neurocomputational science, memristors are often used to simulate electromagnetic radiation or coupled synapse, and most studies have explored the effects of electromagnetic radiation intensity and synaptic coupling strength on neuron firing behavior. However, it is worth noting that the brain is a very powerful information processing center consisting of a large number of neurons and synapses, where different types of synaptic plasticity play an active role in information processing.[45] Consequently, we assert that investigating the role of synaptic plasticity in neurodynamics is essential. Wang *et al*.[46] designed a memristive neural network with plastic synapses and implemented advanced neural activities such as learning, associative memory, and three kinds of forgetting based on the spiking-rate-dependent plasticity rule. Mannan *et al*.[47] proposed a complex neuro-memristive synapse that exhibits short- and long-term plasticity phenomena, the analog characteristics of the artificial synapse were verified by simulating relative biological phenomena. To restore synaptic plasticity in neuronal systems, we mimic the coupling synapse between neurons using a memristor with configurable short-term and long-term plasticity, whose mathematical model can be defined as

$$\begin{cases} i = W(u)v = (e + f\tanh(u))v, \\ \dfrac{\mathrm{d}u}{\mathrm{d}t} = -8u^3 + 2u^2 + 6u - 0.5v - m, \end{cases} \tag{1}$$

where v and i are the input voltage and the output current, $W(u) = e + f\tanh(u)$ is the memductance, e and f are two real paremeters, u is the memristor's internal state. In particular, m is the parameter that controls the memristor to switch between short-term and long-term memories.

2.2. Short-term and long-term plasticity of the memristor

Short-term and long-term plasticity of biological synapses underlie key physiological functions in neural circuits. Zhang *et al.*[48] modeled short and long-term synaptic functions in an amnesia case with volatile and nonvolatile properties. Wu *et al.*[49] modeled short-term and long-term plasticity of synapses in a Pt/HfO_2/Ti memristor by switching between nonvolatile and volatile properties using specific electrical manipulations. The short-term or long-term plasticity of our proposed memristor is controlled by the parameter m. Specifically, we consider the following two cases.

Case (i) When $m = 0$, the power-off plot (POP) of the memristor is shown as the blue trajectory in Fig. 1. It is observed that the POP has three intersections with the x axis, two of which are negative slope intersections, thus the memristor has two asymptotically stable equilibrium points. According to the principle of nonvolatility proposed by Chua:[50] if the POP diagram of a memristor has two or more stable equilibrium points with the x axis, it can be claimed that the memristor has nonvolatility. Therefore, the memristor is nonvolatile in this case and can be used to model the long-term plasticity of coupled synapse.

Case (ii) When $m = 3$, the power-off plot (POP) of the memristor is shown as the red trajectory in Fig. 1. Observe that the POP has only one intersection with the x axis with negative slope, meaning the memristor has only one asymptotically stable equilibrium point. Thus, in this case, the memristor is volatile and can be used to simulate the short-term plasticity of the coupled synapse.

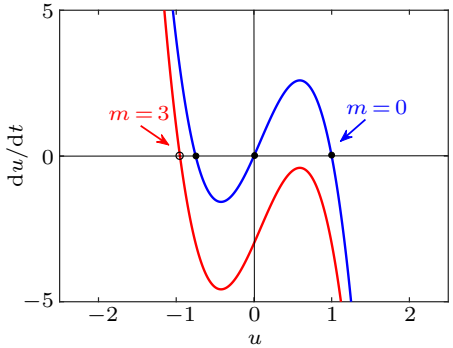


Fig. 1. POP of the memristor with configurable long-term and short-term plasticity.

Synaptic plasticity is mainly due to short-term and long-term mechanisms[51] to simulate synaptic function. Changes in memductance of a memristor can characterize changes in its memory state. In short-term memory, the memductance will decay for a short time after receipt of external stimulus, while in long-term memory, the memductance will remain for a long time after being increased to a fixed value.[52] To reveal the short-term and long-term plasticity of the memristor,[53] a step voltage with the form

$$V_m = \begin{cases} 0\ \text{mV}, & t < 0.5\ \text{s}, \\ 200\ \text{mV}, & t \geq 0.5\ \text{s}, \end{cases} \tag{2}$$

is imposed on it. Fix the initial state of the memristor $u(0) = 0.8$, as shown in Fig. 2(a), the response current marked in red ($m = 3$) increases immediately and then spontaneously decays to a fixed value in a short period of time, thereby forming a brief spike. This spontaneous decay resembles the loss of information, thus indicating the short-term plasticity of the memristive synapse. The blue trace represents the current response of the memristor when it is nonvolatile ($m = 0$). Observe that the response current increases rapidly to a fixed value and then stays in a plateau state, when the step voltage is applied on it. Thus, we can include that the memrsitor can exhibit long-term plasticity when it is nonvolatile. Figure 2(b) illustrates the corresponding memductance evolves over time. It is observed that the initial value of the memductance is 0.82 at $t = 0$. After receiving a step voltage excitation at $t = 0.5$, the red-marked memductance ($m = 3$) undergoes a brief spike before decaying, while the blue-marked memory conductance ($m = 0$) increases rapidly and then remains at a fixed value. Notably, the memductance closely corresponds to changes in response current, further emphasizing both the long-term and short-term plasticity of the memristor.

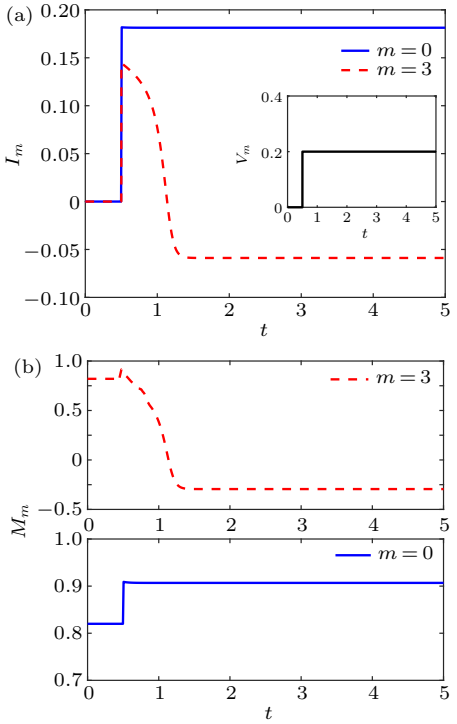


Fig. 2. Short-term and long-term plasticity of the memristor, the red (resp., blue) trajectory corresponds to when the memristor is configured as a volatile (resp., nonvolatile) memristor. (a) The respond current of the memristor, inset shows the input step voltage with $A = 200$ mV. (b) The respond memductance of the memristor.

2.3. Pinched hysteresis loops

Let the memristor parameters $e = 0.3$ and $f = 0.8$ and the initial state $u(0) = 1$, a voltage excitation source $v = A\sin(2\pi Ft)$ is imposed on it to reveal the pinched hysteresis loop characteristics of the memristor with configurable memory. In Fig. 3, the first row illustrates the hysteresis loops of the memristor operating in long-term memory ($m = 0$), and the second row depicts the hysteresis loops of the memristor operating short-term memory ($m = 3$). It can be seen from the figure that all hysteresis loops always pass through the origin, the lobe area is inversely proportional to the excited frequency F and the hysteresis loop finally tends to be a straight line when the excited frequency F surpasses some value. The proposed memristor, thus, satisfies three essential fingerprints whether it operates in short-term or long-term memory.[54]

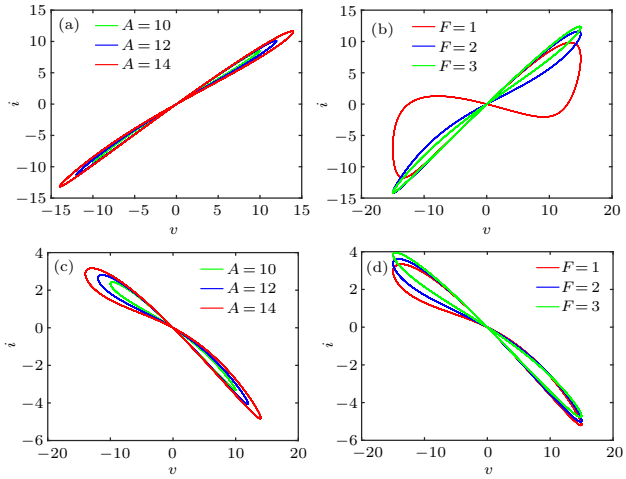


Fig. 3. Pinched hysteresis loops of the memristor. (a) The amplitude-dependent pinched hysteresis loops with $F = 3$ Hz and $u(0) = 1$. (b) The frequency-dependent pinched hysteresis loops with $A = 15$ V and $u(0) = 1$ when the memristor operates in long-term memory. (c) The amplitude-dependent pinched hysteresis loops with $F = 3$ Hz and $u(0) = 1$. (d) The frequency-dependent pinched hysteresis loops $A = 15$ V and $u(0) = 1$ when the memristor operates in short-term memory.

3. Synapse-coupled neuron model under electromagnetic radiation

3.1. Description of the memristor synapse-coupled neuron model

The human brain is an extremely complex dynamic network, and neurons are the basis of brain information processing. The main communication mode between neurons is synaptic transmission. It is worth noting that synaptic connections are dynamic and plastic, and synaptic plasticity affects memory and storage in the brain, which suggests that it is necessary to investigate the influence of synaptic plasticity on information transfer between neurons. In addition, the effect of electromagnetic radiation is also a factor that cannot be ignored in revealing the firing behavior of neurons. Here, the effect of electromagnetic radiation is simulated by an ideal flux-controlled memristor, which is written as

$$\begin{cases} i = W(\phi)v = \phi v, \\ \dfrac{\mathrm{d}\phi}{\mathrm{d}t} = v, \end{cases} \tag{3}$$

where ϕ represents the flux, $W(\phi) = \phi$ is the memductance, v and i are the input voltage and output current.

Using the memristor with configurable short-term and long-term plasticity as the coupling synapse to connect two HR neurons,[5] and two ideal flux-controlled memristors to simulate the electromagnetic induction effects surrounding neurons, a homogeneous neuronal network is developed in Fig. 4 and is formulated as

$$\begin{cases} \dot{x}_1 = y_1 - ax_1^3 + bx_1^2 - \rho(e + f\tanh(u))(x_1 - x_2) + k_1\phi_1 x_1, \\ \dot{y}_1 = c - dx_1^2 - y_1, \\ \dot{x}_2 = y_2 - ax_2^3 + bx_2^2 + \rho(e + f\tanh(u))(x_1 - x_2) + k_2\phi_2 x_2, \\ \dot{y}_2 = c - dx_2^2 - y_2, \\ \dot{u} = (-2u)^3 + 2u^2 + 6u - 0.5(x_1 - x_2) - m, \\ \dot{\phi}_1 = x_1, \\ \dot{\phi}_2 = x_2. \end{cases} \tag{4}$$

In Eq. (4), x_1 and x_2 are the membrane potentials, y_1 and y_2 are recovery variables. $a = 1$, $b = 3$, $c = 1$, $d = 5$ are system parameters of the HR neuron model. u represents the memristive synapse variable and ϕ_1, ϕ_2 are the magnetic fluxes across the membrane. ρ denotes the coupling strength, k_1 and k_2 indicate the electromagnetic radiation intensities.

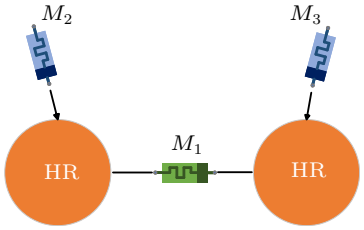


Fig. 4. Memristor-coupled homogeneous neuron network exposed to the external electromagnetic radiation, where the memristor M_1 is considered as the coupled synapse, M_2 and M_3 simulate the effects of electromagnetic radiation.

3.2. Equilibrium points analysis

Setting the left-hand-side of Eq. (4) to zero, the equilibrium points can be determined by

$$\begin{cases} 0 = y_1 - ax_1^3 + bx_1^2 - \rho(e + f\tanh(u))(x_1 - x_2) + k_1\phi_1 x_1, \\ 0 = c - dx_1^2 - y_1, \\ 0 = y_2 - ax_2^3 + bx_2^2 + \rho(e + f\tanh(u))(x_1 - x_2) + k_2\phi_2 x_2, \\ 0 = c - dx_2^2 - y_2, \\ 0 = (-2u)^3 + 2u^2 + 6u - 0.5(x_1 - x_2) - m, \\ 0 = x_1, \\ 0 = x_2. \end{cases} \tag{5}$$

From Eq. (5), it can be seen that $y_1 = 0$ in the first equation since $x_1 = x_2 = 0$, which contradicts the second equation with $y_1 = c > 0$. In addition, the third equation $y_2 = 0$ and the

fourth equation $y_2 = c > 0$ are also contradictory. Therefore, equation (5) lacks a real solution, meaning system (4) has no equilibrium point and the generated attractors are hidden.[55]

4. Dynamics analysis of the neuron network

4.1. Dynamics related to coupling strength ρ

In the following analysis, we explore the effect of the synaptic plasticity on the dynamics of the neuronal network system. First, we use the coupling strength ρ as the bifurcation parameter, the other system parameters are fixed as $a = 1$, $b = 3$, $c = 1$, $d = 5$, $e = 0.3$, $f = 0.8$, $k_1 = 0.06$, $k_2 = 0.65$, and the seven initial values of the neuron network are specified as (0, 1, 0, 0, 1, 1, 1). The bifurcation diagrams of the membrane potential x_1 and the first two Lyapunov exponents with respect to the coupling strength ρ are depicted in Figs. 5 and 7 with different plasticity of memristive synapse. When the memristive synapse is configured as long-term plasticity ($m = 0$), the bifurcation diagram and the first two Lyapunov exponents are depicted in Figs. 5(a) and 5(b). Observe that the network evolves from chaotic firing to a period-2 firing through an anti-period-doubling bifurcation route. The phase diagrams and time series of chaotic firing, period-8, period-4, and period-2 firing at $\rho = 0.5$, 0.68, 0.86, and 1.2 are plotted in Fig. 6, which demonstrates the above anti-period-doubling bifurcation scenario. When the memristor is configured as short-term plasticity ($m = 3$), the network exhibits totally different bifurcation behaviors. According to the bifurcation diagram and the first two Lyapunov exponents in Figs. 7(a) and 7(b), one can find that the network transits from period-2 firing to chaotic firing via a forward period-doubling bifurcation scenario. Similarly, four sampled phase diagrams and time series at $\rho = -4$, -2.5, -2.1, and -1.6, as shown in Fig. 8, demonstrate that the neuronal network transits from period-2 to period-4 firing, then to period-8 firing and finally to chaotic firing as the coupling strength ρ increases, which intuitively reflect the forward period-doubling bifurcation scenario. Comparing Fig. 5 with Fig. 7, one can find that the neuronal network exhibits the opposite bifurcation routes when the memristive synapse is configured as different memory attributes. Thus, the synaptic plasticity of the memristive synapse has a great impact on the firing activities of the neuronal network.

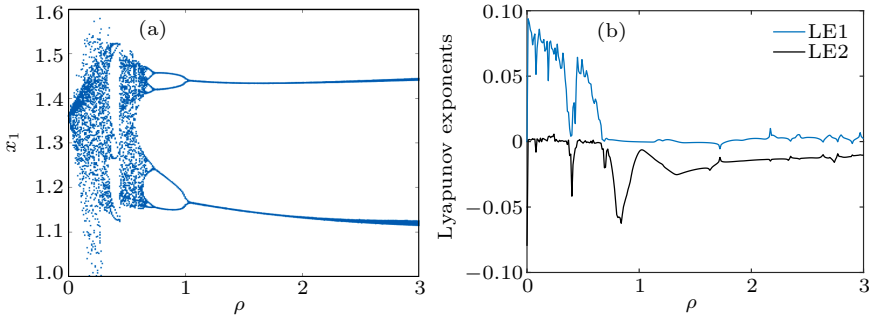


Fig. 5. Bifurcation diagrams (a) and the first two Lyapunov exponents (b) with respect to ρ, when the memristor (1) operates in long-term memory ($m = 0$).

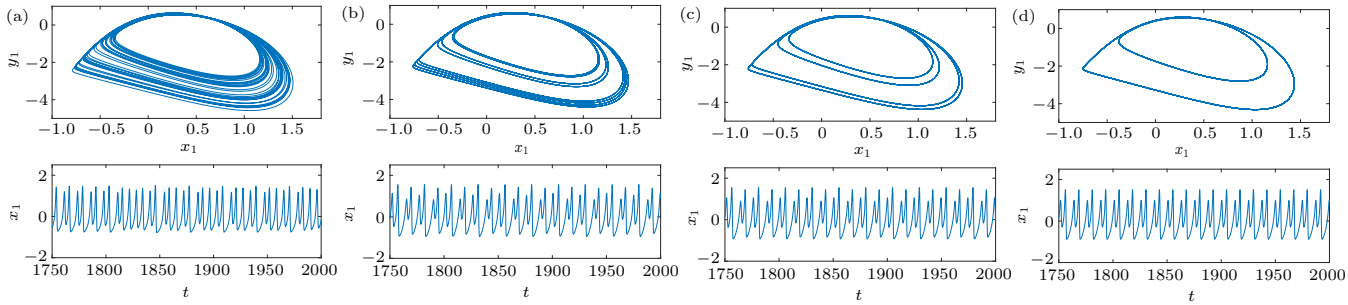


Fig. 6. Long-term synaptic plasticity induces firing pattern transitions ($m = 0$): (a) chaotic firing with $\rho = 0.5$, (b) period-8 firing with $\rho = 0.68$, (c) period-4 firing with $\rho = 0.86$, (d) period-2 firing with $\rho = 1.2$.

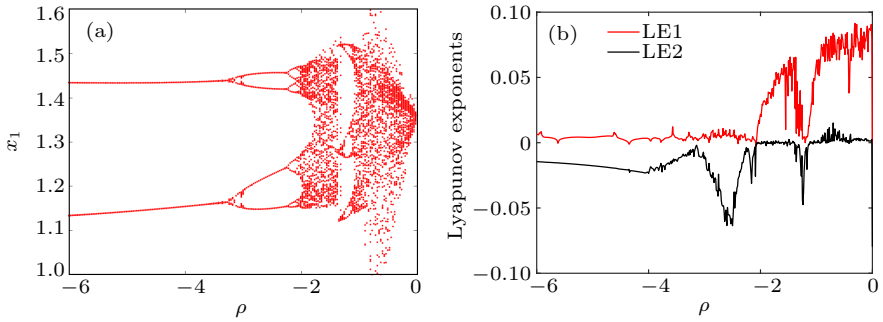


Fig. 7. Bifurcation diagrams (a) and the first two Lyapunov exponents (b) with respect to ρ, when the memristor (1) operates in short-term memory ($m = 3$).

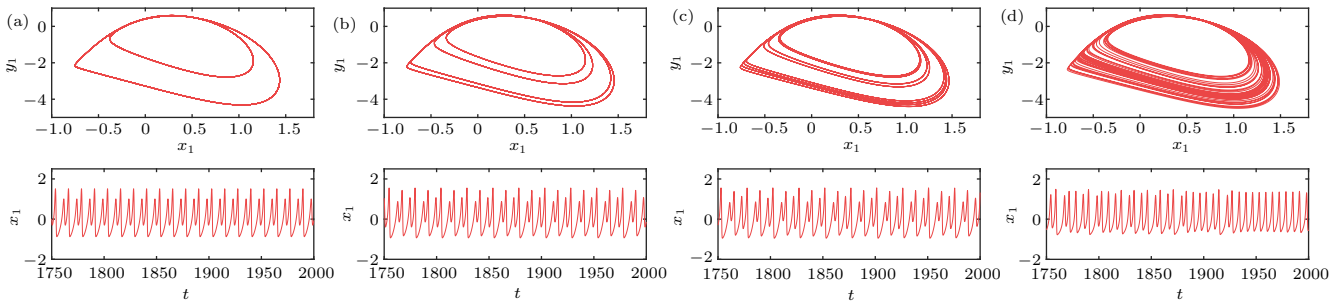


Fig. 8. Short-term synaptic plasticity induces firing pattern transitions ($m = 3$): (a) period-2 firing with $\rho = -4$, (b) period-4 firing with $\rho = -2.5$, (c) period-8 firing with $\rho = -2.1$, (d) chaotic firing with $\rho = -1.6$.

4.2. Effect of electromagnetic radiation strengths

We have previously explored the effects of synaptic coupling strength ρ on the firing behavior of neuron network. In this subsection, we focus on the effect of electromagnetic radiation on the firing activities of neural network. Let the coupling strength $\rho = 1$ and the other parameters remain unchanged. When the electromagnetic radiation strengths k_1 and k_2 are considered as the two control parameters, the 2D dynamic maps are obtained as shown in Figs. 9(a), and 9(b) for $m = 0$ and $m = 3$, respectively. Note that period-1 to period-8 firing are represented in different colors marked with numbers '1' to '8', when the firing period is greater than 9, the network exhibits chaotic firing which marked by CH. Thus, the 2D dynamic maps clearly reflect the firing patterns and firing period under different electromagnetic radiation. Comparing Fig. 9(a) with Fig. 9(b), one can observe that the parameter space for periodic firing in the presence of long-term memory synapse is significantly broader than that in the presence of short-term memory synapse. This intuitively suggests that the synaptic plasticity plays an important role in the firing behavior of neural networks.

To better elucidate the effect of the synaptic plasticity on the firing activity of the neuron network, let the coupling strength $\rho = 1$ and the electromagnetic radiation intensity $k_1 = 0.3$, the other parameters remain unchanged. When the memristive synapse operates in long-term memory, the bifurcation diagram and the first two Lyapunov exponents with respect to the parameter k_2 are plotted in Figs. 10(a) and 10(b). Observe that the neuron network exhibits periodic firing in the interval $k_2 \in [0\ 0.7]$ and then it undergoes tangential bifurcation, leading to chaotic firing. Figures 11(a)–11(d) plot the phase portraits and time series diagrams of period-1, period-2, period-4, and chaotic firing at $k_2 = 0.1$, 0.33, 0.48, and 0.8, respectively. When the network is affected by short-term synaptic plasticity ($m = 3$), its firing behavior alters. As demonstrated in Figs. 12(a) and 12(b), the network initially experiences an anti-period-doubling bifurcation, transitioning from period-2 firing to period-1 firing, and ultimately evolves into chaotic firing through a forward period-doubling bifurcation. Similarly, four sampled phase diagrams and time series at $k_2 = 0.2$, 0.36, 0.42, and 0.8 are depicted in Fig. 13.

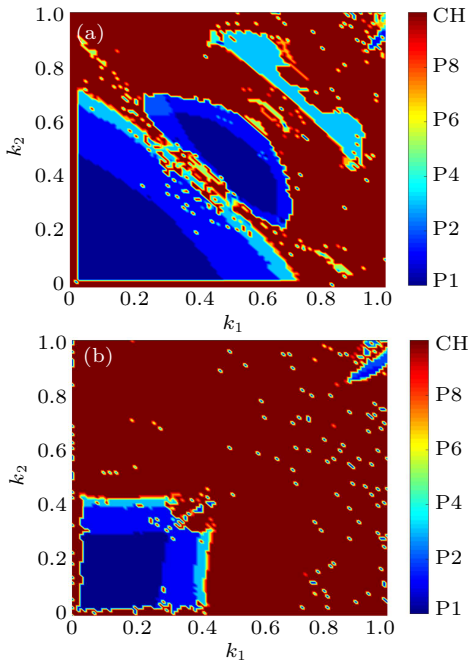


Fig. 9. The 2D dynamic map related to k_1 and k_2 under different values of m: (a) $m = 0$ and (b) $m = 3$.

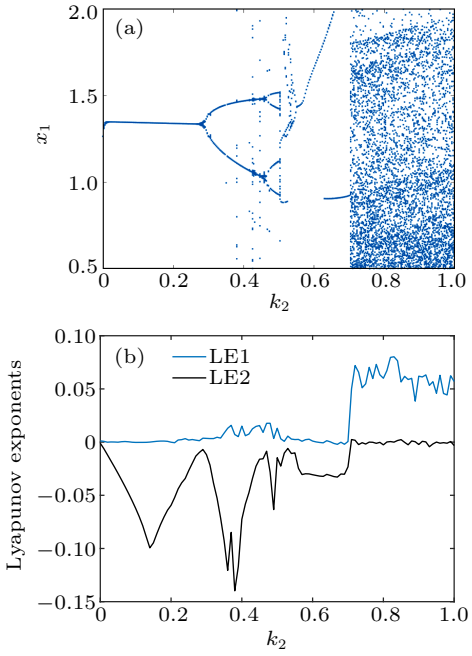


Fig. 10. Bifurcation diagrams (a) and the first two Lyapunov exponents (b) with respect to k_2, when the memristor (1) is configured as a non-volatile memristor ($m = 0$).

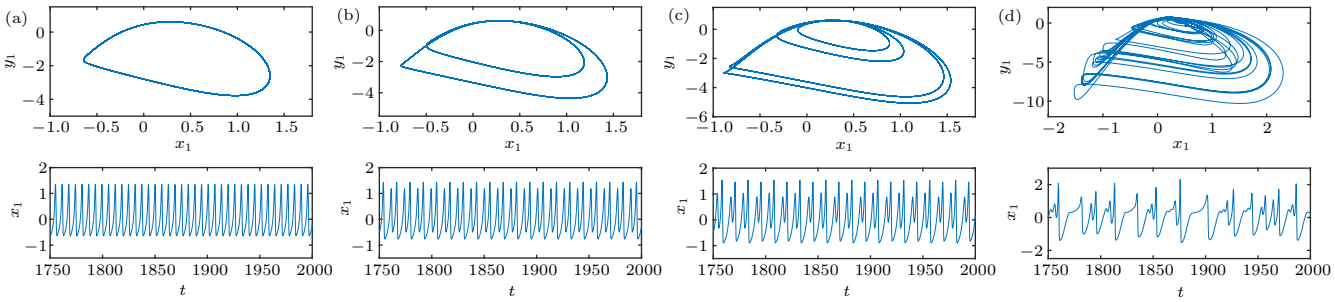


Fig. 11. Long-term synaptic plasticity induces firing pattern transitions ($m = 0$): (a) period-1 with $k_2 = 0.1$, (b) period-2 firing with $k_2 = 0.33$, (c) period-4 firing with $k_2 = 0.48$, (d) chaotic firing with $k_2 = 0.8$.

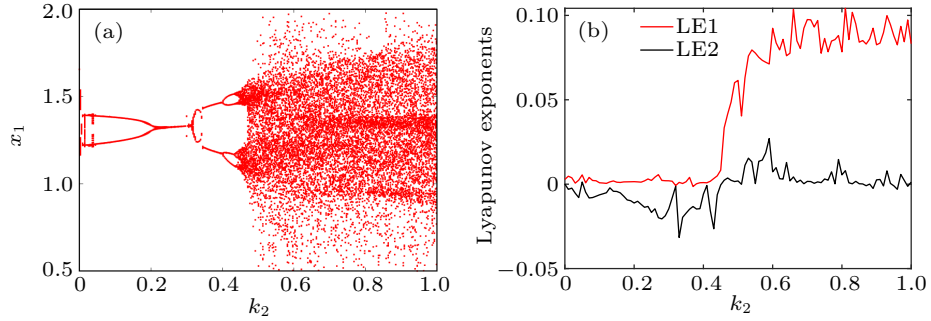


Fig. 12. Bifurcation diagrams (a) and the first two Lyapunov exponents (b) with respect to k_2, when the memristor (1) is configured as a volatile memristor ($m = 3$).

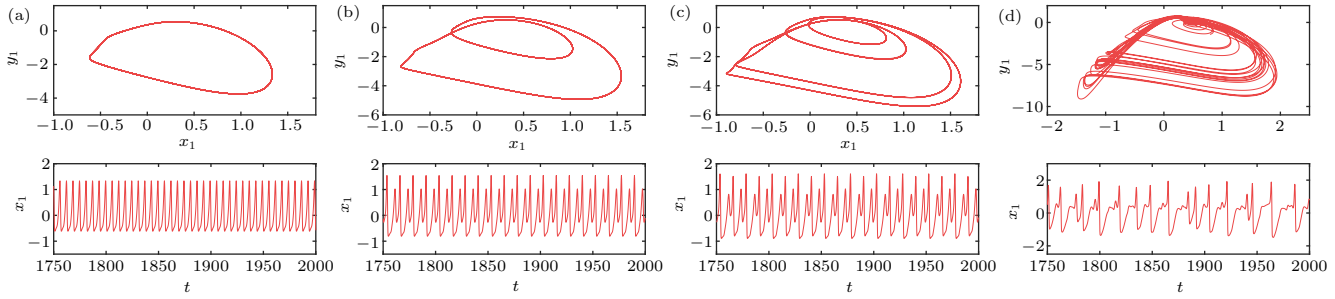


Fig. 13. Short-term synaptic plasticity induces firing pattern transitions ($m = 3$): (a) period-1 with $k_2 = 0.28$, (b) period-2 firing with $k_2 = 0.36$, (c) period-4 firing with $k_2 = 0.42$, (d) chaotic firing firing with $k_2 = 0.8$.

5. Synchronous behaviors under different coupling strengths

Synchronization is a key feature of brain dynamics that is necessary for achieving advanced brain functions such as cognition, learning, and memory.[56] Pathologically synchronous firing of neurons leads to many neurological and psychiatric disorders such as Parkinsonian symptoms and epileptic seizures.[57] Synaptic plasticity can greatly influence the synchronized behavior of neuronal networks.[58] In the following, we focus on the effect of synaptic plasticity on the synchronization behavior of the network by adjusting the coupling strength.

The definition of a burst phase must be illustrated, which is expressed as[59]

$$\theta(t) = 2\pi n + 2\pi \frac{t - t_n}{t_{n+1} - t_n}, \quad (t_n < t < t_{n+1}), \tag{6}$$

where t_n is the time when the n-th cluster occurs, $t_{n+1} - t_n$ means the interburst interval. From Eq. (6), it can be seen that each burst generation is accompanied by a phase increase of 2π. The phase variable $\theta(t)$ can capture the time series characteristics of the neuron's membrane potential or firing activity.[59] In order to avoid negative values interfering with the analysis, the absolute value of the phase difference between two neurons is usually expressed as $|\Delta\theta(t)|$. The phase synchronization between two neurons occurs when the phase difference $|\Delta\theta(t)| = |\theta_1(t) - \theta_2(t)|$ is bounded with the value of 2π.

Let the system parameters $a = 1$, $b = 3$, $c = 1$, $d = 5$, $e = 0.3$, $f = 0.8$, $k_1 = 0.2$, $k_2 = 0.5$, and the initials are selected as (0, 1, 0, 0, 1, 1, 1). When the memristive synapse is configured as long-term plasticity ($m = 0$), the time series of membrane potentials x_1, x_2, and their phase difference are shown in Fig. 14. At $\rho = 0.1$, as illustrated in Figs. 14(a) and 14(b) the two neurons are desynchronized since their phase difference is much larger than 2π. When ρ increases to 0.7, the phase difference fluctuates around 6.2, indicating the two neurons are close to phase synchronization (see Figs. 14(c) and 14(d)).

While at $\rho = 1.1$, the phase difference fluctuates around 0, as shown in Fig. 14(f). In this case, from Fig. 14(e), one can find that the timing of the action potentials of the two neurons is consistent with each other, suggesting complete phase synchronization is achieved.

When the memristive synapse is configured as short-term plasticity with $m = 3$, and the other parameters remain unchanged, the synchronization transition behavior is shown in Fig. 15. Figures 15(a) and 15(b) depict the desynchronized behavior of the two neurons at $\rho = -0.1$. At $\rho = -0.7$, the two neurons are approximated to phase synchronization, as illustrated to Figs. 15(c) and 15(d). Finally, the two neurons are achieved complete phase synchronization at $\rho = -1.1$ with the phase difference being 0 (see Figs. 15(e) and 15(f)).

It can be seen that the greater the absolute value of the coupling strength ρ, the easier it is for two neurons to achieve phase synchronization. It is worth noting that in the case of long-term synaptic plasticity, the two neurons gradually achieve phase synchronization as the coupling strength ρ increases along the positive direction. In contrast, in the case of short-term synaptic plasticity, neurons gradually synchronize as ρ increases in the opposite direction.

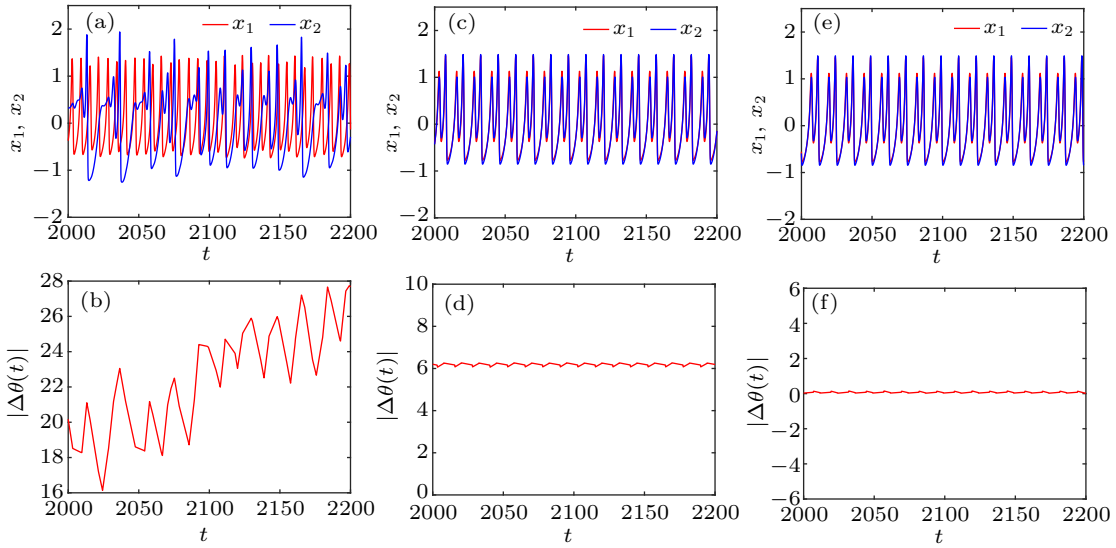


Fig. 14. The effect of the coupling strength ρ on phase synchronization of the coupled neurons during long-term synaptic plasticity ($m = 0$): (a)–(b) $\rho = 0.1$, (c)–(d) $\rho = 0.7$, (e)–(f) $\rho = 1.1$. In the figure, panels (a), (c), and (e) are time sequences of membrane potentials, panels (b), (d), and (f) denote the absolute value of the phase different between two neurons.

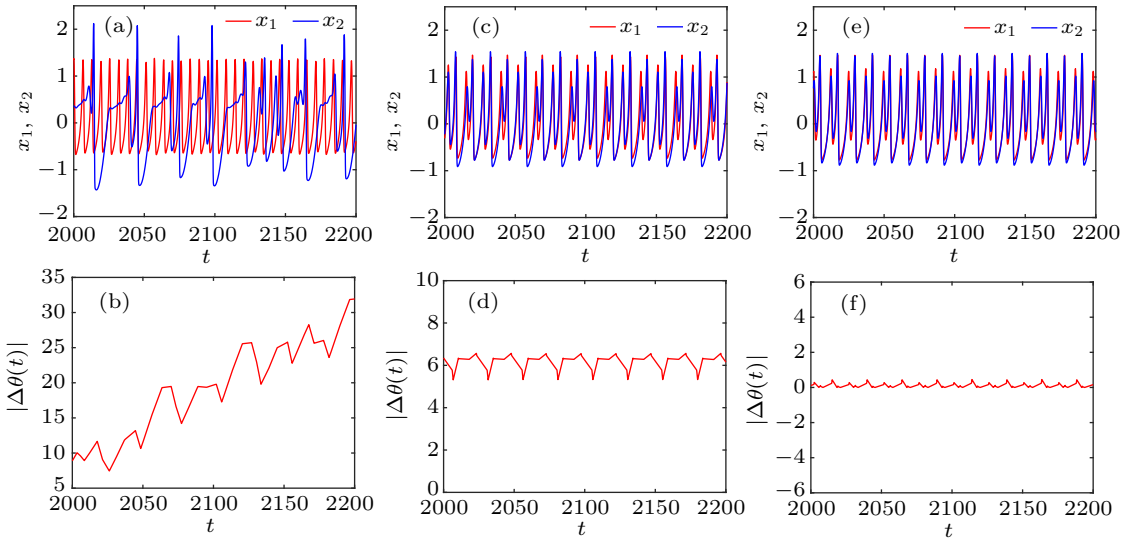


Fig. 15. The effect of the coupling strength ρ on phase synchronization of the coupled neurons during long-term synaptic plasticity ($m = 3$): (a)–(b) $\rho = -0.1$, (c)–(d) $\rho = -0.7$, (e)–(f) $\rho = -1.1$. Panels (a), (c), and (e) are time sequences of membrane potentials, panels (b), (d), and (f) denote the absolute value of the phase different between two neurons.

6. Digital hardware experiments

In this section, we develop an MCU-based hardware platform to implement the proposed 7D neuron network model. Compared to analog circuits, microcontroller-based digital circuits are programmable, compact, and flexible in analyzing the parameters and initial conditions of nonlinear dynamical systems, since they can be accurately preconfigured by software.[60] The STM32 hardware board mainly includes one

STM32F407ZGT6 microcontroller, two 16-bit DAC8563 converters, and two interface level switching circuits. On the hardware board, by capturing the signals with an oscilloscope, we verify the hidden attractors and time series of the network system. In order to digitally implement the proposed neuron network, we use Euler method to obtain a discrete-time model according to system (4) as follows:

$$\begin{aligned}
x_{1,n+1} &= x_{1,n} + h(y_{1,n} - ax_{1,n}^3 + bx_{1,n}^2 \\
&\quad - \rho(e + f\tanh(u_{1,n}))(x_{1,n} - x_{2,n}) + k_1\phi_{1,n}x_{1,n}), \\
y_{1,n+1} &= y_{1,n} + h(c - dx_{1,n}^2 - y_{1,n}), \\
x_{2,n+1} &= x_{2,n} + h(y_{2,n} - ax_{2,n}^3 + bx_{2,n}^2 \\
&\quad + \rho(e + f\tanh(u_{1,n}))(x_{1,n} - x_{2,n}) + k_2\phi_{2,n}x_{2,n}), \\
y_{2,n+1} &= y_{2,n} + h(c - dx_{2,n}^2 - y_{2,n}), \\
u_{1,n+1} &= u_{1,n} + h((-2u_{1,n})^3 + 2u_{1,n}^2 \\
&\quad + 6u_{1,n} - 0.5(x_{1,n} - x_{2,n}) - m), \\
\phi_{1,n+1} &= \phi_{1,n} + h(x_{1,n}), \\
\phi_{2,n+1} &= \phi_{2,n} + h(x_{2,n}),
\end{aligned} \tag{7}$$

where $h = 0.01$ denotes the step size. The discrete-time model of the network is programmed in C language and then downloaded to the STM32 hardware board. The system parameters and initial conditions are accurately preset corresponding to the corresponding numerical results. Then, turn on the power, run the program, and synchronously output the dual channel analog voltage sequences to the oscilloscope. The captured phase portraits and the corresponding time series of the neurons coupled by the long-term memory memristive synapse are displayed in Figs. 16(a)–16(d), which are consistent with the numerical simulation results in Figs. 6(a)–6(d). Figures 17(a)–17(d) are the captured results when the memristive synapse operates in short-term memory, which closely match the numerical results in Figs. 8(a)–8(d).

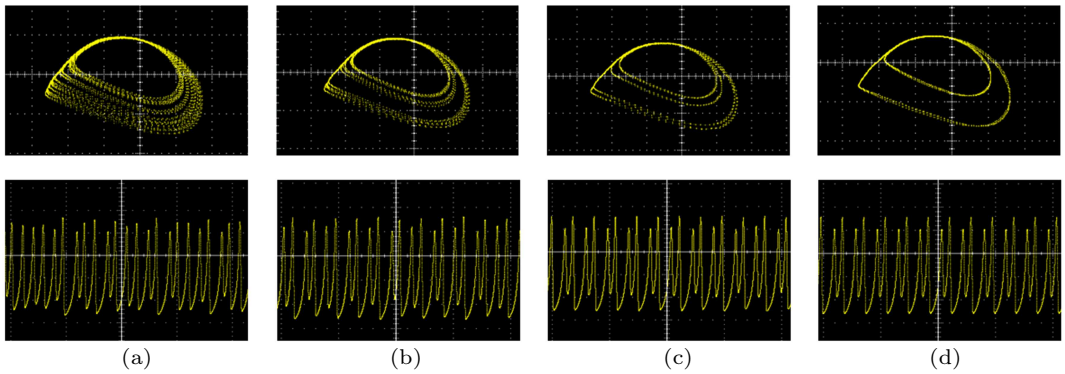


Fig. 16. Hardware experimental results obtained with oscilloscope when the memristive synapse operates in long-term memory: (a) chaotic firing, (b) period-8 firing, (c) period-4 firing, (d) period-2 firing.

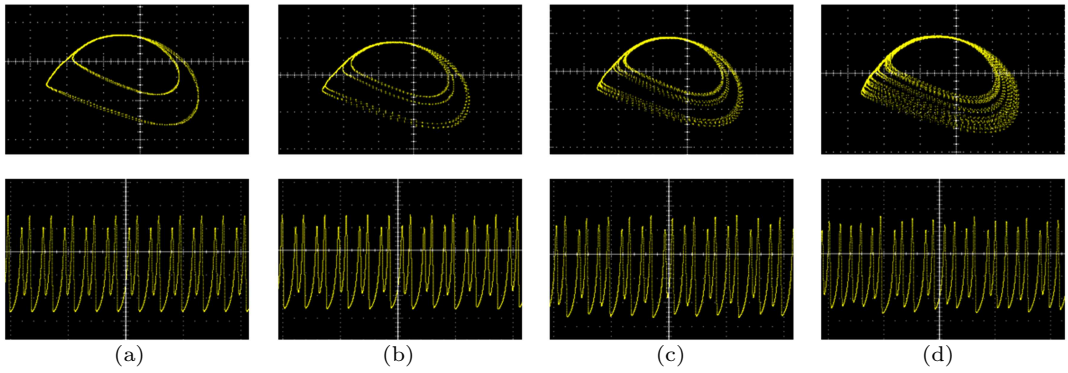


Fig. 17. Hardware experimental results obtained with oscilloscope when the memristive synapse operates in short-term memory: (a) period-2 firing, (b) period-4 firing, (c) period-8 firing, (d) chaotic firing.

7. Conclusion

To reveal the effect of synaptic plasticity on neuron networks, a memristor has been proposed in this study to realize short-term and long-term plasticity by changing its control parameter. A bi-neuron network then has been developed with the proposed memristor acting as the coupling synapse and the effect of electromagnetic induction being simulated by the ideal flux-controlled memristors. Although the presented neuron network has no equilibrium point, it can exhibit complex hidden firing activities, which has been revealed by numerical analysis methods such as phase diagram, time series, bifurcation diagram, Lyapunov exponent, and 2D dynamic maps. The obtained results show the long-term and short-term plasticity of the memristive synapse can induce different bifurcation scenarios as the coupling strength varies. In addition, the long-term plasticity of the memristive synapse evokes periodic

firing in broader parameter space than its short-term plasticity. In particular, regardless of whether the synaptic coupling is characterized by long-term or short-term plasticity, as the coupling strength increases in the opposite direction, the two neurons gradually synchronize. Finally, a hardware system was constructed based on the STM32 microcontroller, and some experimental results were provided to verify the correctness of the numerical simulation. It is hoped that our study will further understand the effects of long-term and short-term plasticity of memristive synapses on the firing activity of neuronal networks.

Acknowledgement

Project supported by the National Natural Science Foundations of China (Grant Nos. 62171401 and 62071411).

References

[1] Xu F, Zhang J, Fang T, Huang S and Wang M 2018 *Nonlinear Dyn.* **92** 1395
[2] Dias C, Castro D, Aroso M, Ventura J and Aguiar P 2022 *ACS Appl. Electron. Mater.* **4** 2380
[3] Mariano P M and Spadini M 2024 *Physica D* **458** 133993
[4] Hodgkin A L and Huxley A F 1952 *J. Physiol.* **117** 500
[5] Hindmarsh J L and Rose R M 1982 *Nature* **296** 162
[6] Izhikevich E M 2003 *IEEE Trans. Neural Network* **14** 1569
[7] Izhikevich E M 2006 *Scholarpedia* **1** 1349
[8] Huang L, Wang S, Lei T, Huang K and Li C 2024 *Int. J. Bifurcat. Chaos* **34** 2450022
[9] Njitacke Z T, Kengne J and Fotsin H B 2019 *Int. J. Dyn. Control* **7** 36
[10] Lai Q, Wan Z, Zhang H and Chen G 2023 *IEEE Trans. Neural Networks Learn. Syst.* **34** 7824
[11] Zhang S, Zheng J, Wang X and Zeng Z 2021 *Chaos, Solitons and Fractals* **145** 110761
[12] Ge M, Xu Y, Lu L, Zhao Y, Yang L, Zhan X and Jia Y 2018 *IET Syst. Biol.* **12** 177
[13] Wu K, Wang T, Wang C, Du T and Lu H 2018 *Neural Comput. Appl.* **30** 551
[14] Li Z and Chen K 2023 *Chaos, Solitons and Fractals* **175** 114017
[15] Chua L 1971 *IEEE Trans. Circuit Syst.* **18** 507
[16] Innocenti G, Tesi A, Di Marco M and Forti M 2022 *Emerging Sel. Top. Circuits Syst.* **12** 735
[17] Ascoli A, Slesazeck S, Mähne H, Tetzlaff R and Mikolajick T 2015 *IEEE Trant. Circuits-I* **62** 1165
[18] Bao H, Chen M, Wu H G and Bao B C 2020 *Sci. China-Technol. Sci.* **63** 603
[19] Li C L, Li Z Y, Feng W, Tong Y N, Du J R and Wei D Q 2019 *AEU-INT J. Electron. C* **110** 152861
[20] Bao B, Peol M A, Bao H, Chen M, Li H and Chen B 2021 *Chaos, Solitons and Fractals* **144** 110744
[21] Du C, Liu L, Zhang Z and Yu S 2021 *Chaos, Solitons and Fractals* **148** 111023
[22] Chen M, Luo X, Suo Y, Xu Q and Wu H 2023 *Nonlinear Dyn.* **111** 7773
[23] Ma M L, Xie X H, Yang Y, Li Z J and Sun Y C 2023 *Chin. Phys. B* **32** 058701
[24] Peng C, Li Z J, Wang M J and Ma M L 2023 *Nonlinear Dyn.* **111** 16527
[25] Yu X, Bao H, Chen M and Bao B C 2023 *Chaos, Solitons and Fractals* **171** 113442
[26] Bao H, Yu X, Zhang Y, Liu X and Chen M 2023 *Chaos, Solitons and Fractals* **177** 114167
[27] Chen M, Luo X, Suo Y, Xu Q and Wu H 2023 *Nonlinear Dyn.* **111** 7773
[28] Lin H, Wang C, Sun J, Zhang X, Sun Y and Iu H H 2023 *Chaos, Solitons and Fractals* **166** 112905
[29] Takembo C N, Mvogo A, Ekobena Fouda H P and Kofané T C 2019 *Nonlinear Dyn.* **95** 1067
[30] Vinaya M and Ignatius R P 2019 *Int. J. Mod. Phys. C* **30** 1950047
[31] An X, Xiong L, Shi Q, Qiao S and Zhang L 2023 *Nonlinear Dyn.* **111** 9509
[32] Lai Q and Yang L 2024 *Chaos* **34** 013145
[33] Vinaya M and Ignatius R P 2020 *Nonlinear Dyn.* **101** 2369
[34] Kourosh-Arami M, Komaki A, Gholami M, Marashi S H and Hejazi S 2023 *J. Physiol. Sci.* **73** 33
[35] Magee J C and Grienberger C 2020 *Annu. Rev. Neurosci.* **43** 95
[36] Sargsyan A R, Melkonyan A A, Papatheodoropoulos C, Mkrtchian H H and Kostopoulos G K 2003 *Neural Networks* **16** 1161
[37] Oner M, Cheng P T, Wang H Y, Chen M C and Lin H 2024 *Biochem. Biophys. Res. Commun.* **710** 149874
[38] Madadi Asl M, Valizadeh A and Tass P A 2018 *Sci. Rep.* **8** 12068
[39] Madadi Asl M and Ramezani Akbarabadi S 2021 *Plos One* **16** e0257228
[40] Madadi Asl M and Ramezani Akbarabadi S 2023 *Cogn. Neurodynamics* **17** 523
[41] Chen L, Li C, Huang T, Chen Y, Wen S and Qi J 2013 *Phys. Lett. A* **377** 3260
[42] Zhou W, Wen S, Liu Y, Liu L, Liu X and Chen L 2023 *Neural Networks* **158** 293
[43] Chen L, Zhou W, Li C and Huang J 2021 *Neurocomputing* **456** 126
[44] Zhang J and Li Z J 2024 *Nonlinear Dyn.* **112** 6647
[45] Li C, Zhang X, Chen P, Zhou K, Yu J and Wu G 2023 *iScience* **26** 106315
[46] Wang Y, Wang G, Shen Y and Iu H H C 2020 *Circuits Syst. Signal Process* **39** 3496
[47] Mannan Z I, Kim H and Chua L 2021 *Sensors* **21** 644
[48] Zhang X, Liu S, Zhao X, Wu F, Wu Q and Wang W 2017 *IEEE Electron Dev. Lett.* **38** 1208
[49] Wu L, Liu H, Lin J and Wang S 2021 *IEEE Trans. Electron Dev.* **68** 1622
[50] Chua L 2018 *Appl. Phys. A* **124** 563
[51] Deperrois N and Graupner M 2020 *PLoS Comput. Biol.* **16** e1008265
[52] Wen L and Ong C K 2024 *Int. J. Bifurcation Chaos* **34** 2450040
[53] Shakib M A, Gao Z and Lamuta C 2023 *ACS Appl. Electron. Mater.* **5** 4875
[54] Chua L 2014 *Semicond. Sci. Technol.* **29** 104001
[55] Dudkowski D, Jafari S, Kapitaniak T, Kuznetsov N V, Leonov G A and Prasad A 2016 *Phys. Rep.* **637** 1
[56] Shavikloo M, Esmaeili A, Valizadeh A and Madadi Asl M 2023 *Cogn. Neurodynamics* **18** 631
[57] Schmalz J and Kumar G 2019 *Front. Comput. Neurosci.* **13** 61
[58] Hu X, Jiang B, Chen J and Liu C 2022 *Eur. Phys. J. Plus* **137** 895
[59] Wang H X, Lu Q S and Shi X 2010 *Chin. Phys. B* **19** 060509
[60] Njitacke Z T, Tsafack N, Ramakrishnan B, Rajagopal K, Kengne J and Awrejcewicz J 2021 *Chaos, Solitons and Fractals* **153** 111577